Phase behavior of a binary fluid mixture of quadrupolar molecules

Masatoshi Toda, Shinji Kajimoto, Shuichi Toyouchi, Toshihiro Kawakatsu, Yohji Akama, Motoko Kotani, and Hiroshi Fukumura

Phys. Rev. E **94**, 052601 — Published 2 November 2016

DOI: 10.1103/PhysRevE.94.052601

Phase behavior of a binary fluid mixture of quadrupolar molecules

Masatoshi Toda,[1,*] Shinji Kajimoto,[1] Shuichi Toyouchi,[1]
Toshihiro Kawakatsu,[2] Yohji Akama,[3] Motoko Kotani,[3,4] and Hiroshi Fukumura[1]

[1] *Department of Chemistry, Tohoku University, Sendai, 980-8578, Japan*
[2] *Department of Physics, Tohoku University, Sendai, 980-8578, Japan*
[3] *Mathematical Institute, Tohoku University, Sendai, 980-8578, Japan*
[4] *WPI-AIMR, Tohoku University, Sendai, 980-8577, Japan*

(Dated: October 10, 2016)

We propose a model molecule to investigate microscopic properties of a binary mixture with a closed-loop coexistence region. The molecule is comprised of a Lennard-Jones particle and a uniaxial quadrupole. Gibbs ensemble Monte Carlo simulations demonstrate that the high-density binary fluid of the molecules with the quadrupoles of the same magnitude but of the opposite signs can show closed-loop immiscibility. We find that an increase in the magnitude of the quadrupoles causes a shrinkage of the coexistence region. Molecular dynamics simulations also reveal that aggregates with two types of molecules arranged alternatively are formed in the stable one-phase region both above and below the coexistence region. String structures are dominant below the lower critical solution temperature, while branched aggregates are observed above the upper critical solution temperature. We conclude that the anisotropic interaction between the quadrupoles of the opposite signs plays a crucial role in controlling these properties of the phase behavior.

PACS numbers: 64.75.Gh, 82.30.Rs, 61.20.Qg, 05.20.Jj

I. INTRODUCTION

Phase behavior of multicomponent mixtures is one of the key issues in condensed matter research [1]. When we are to understand the mechanism of the phase behavior, among various phase diagrams, those of binary fluid mixtures are of fundamental importance because they are easy to control and analyze. We show typical temperature–composition phase diagrams observed in binary liquids in Fig. 1. The apexes on these phase coexistence curves are the critical points. Based on the position of the critical points on the phase diagram, these phase diagrams can be classified into three types: Fig. 1 (a) the upper critical solution temperature (UCST) type, (b) the lower critical solution temperature (LCST) type, and (c) closed-loop type that has the characters of both UCST and LCST-type phase diagrams. Although most binary liquids show the UCST-type phase diagram, there is a certain group of mixtures that show the LCST-type phase diagram. Water–phenol and hexane–nitrobenzene systems are examples of the former type, while water–triethylamine and water–1-ethylpiperidine systems are ones of the latter type [2]. Examples of the remaining closed-loop type are rather few but have a special importance as a prototype system to study both UCST and LCST-type phase behaviors in a unified manner. Nicotine–water mixture is a typical example of this category [2, 3]. From a scientific point of view, such a closed-loop phase diagram is a manifestation of the re-entrant phase transition [4], which has been a target of intensive studies in the fields of colloidal science [5], protein science [6], and high energy physics [7]. From an engineering one, on the other hand, understanding the differences in the microscopic behavior between UCST and LCST is also crucial in controlling the phase separation phenomena in chemical processing.

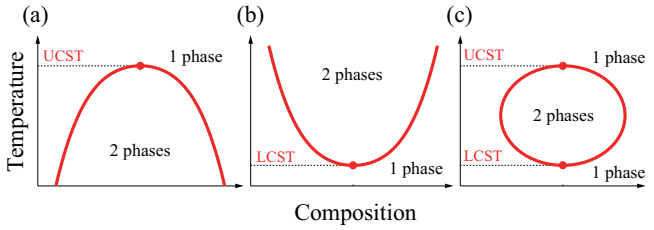

FIG. 1. (Color online) Three temperature–composition phase diagrams often observed in binary liquids: (a) UCST-type, (b) LCST-type, and (c) closed-loop-type (LCST < UCST) phase diagrams. In each diagram, the red curve is the phase coexistence curve, *i.e.*, the binodal curve, and the apex(es) on the curve is(are) the critical point(s). Thermodynamically, the binary liquid separates into two phases in the region labeled "2 phases," while it is homogeneous in the region labeled "1 phase."

The phase behavior near the UCST of a binary mixture can be explained by the balance between the entropy of mixing of the two components and the van der Waals attractive interaction between similar species. On the other hand, the phase behavior near the LCST is more complicated than that near the UCST and is still not well understood. As far as low-molecular systems are concerned, it is known that the behavior is related to an entropy effect associated with molecular orientations

* Present affiliation: National Institute of Advanced Industrial Science and Technology (AIST), Tsukuba 305-8568, Japan; Electronic mail: m.toda@aist.go.jp

caused by anisotropic intermolecular interactions [4, 8]. At low temperatures, specifically, the anisotropic interactions form molecular complexes composed of different species, which exist in the spatially homogeneous one-phase state below the LCST. Anisotropic interactions such as hydrogen bond also play a key role in the formation of self-organized structures observed in condensed matter [9]. Hence, understanding molecular details of the behavior of liquids with the anisotropic interactions is one of the central issues of materials science. Based on the above idea, previous studies have adopted a short-ranged anisotropic interaction between different species into their models [10–12], with which they succeeded in reproducing the closed-loop phase diagram. As these existing studies have been carried out with on-lattice-based structures and/or spatially discretized anisotropic interactions, however, the shape and the statistical properties of the molecular complexes at temperatures below the LCST can be artifacts of the discretizations assumed in their models.

The purpose of the present study is to uncover molecular-scale properties of binary liquids with a closed-loop coexistence region using an off-lattice molecular model which is more realistic than the previous models. For this purpose, we propose a minimal model molecule that is free from the lattice discreteness. Our model molecule is an anisotropic molecule that consists of only two elements: a Lennard-Jones (LJ) particle and a uniaxial quadrupole. It is important here to note that we succeeded in reproducing the LCST-type phase diagram by using molecules with electric quadrupoles but without electric dipoles. Because real molecules such as water and triethylamine that show LCST-type phase diagram usually have a permanent electric dipole in addition to quadrupoles and higher multipoles, it has not been clear whether the electric dipole is the origin of the LCST-type phase diagram or not. Thus, our model system can serve as a counter-example to the common idea that the LCST-type and the closed-loop-type phase diagrams are caused by anisotropic interactions due to the electric dipoles. From the standpoint of multipole–multipole interactions, in this study, we examine the phase behavior of our binary mixtures and discuss a condition for the occurrence of the lower critical point or the closed-loop coexistence region. We carry out molecular simulations on the high-density binary mixture of the quadrupolar molecules using two techniques, *i.e.*, the Gibbs ensemble Monte Carlo (GEMC) method [13–15] and the molecular dynamics (MD) method. Our results show that the anisotropic interaction between the quadrupoles of the opposite signs is a key factor in the realization of a closed-loop coexistence region and that the dipole–dipole interaction is not necessary for the occurrence of the lower critical point.

The rest of this paper is organized as follows: We present our model molecules in Sec. II and describe important parts of the used simulation methods, *i.e.*, GEMC and MD, in Sec. III. We show the results obtained from the GEMC simulations in Sec. IV and those from the MD simulations in Sec. V. In the former section, we discuss the phase behavior and a condition for the occurrence of the lower critical point from the viewpoint of multipole–multipole interaction between the constituent molecules. In the latter section, on the other hand, we discuss structural properties in stable one-phase states outside the closed-loop coexistence region. Finally, we conclude the present study with a brief summary and outlook in Sec. VI.

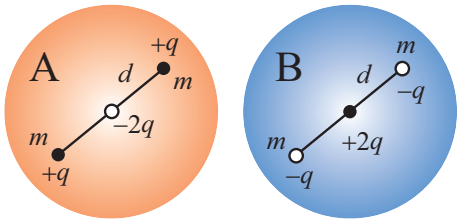

FIG. 2. (Color online) Each of our model molecules A and B is a Lennard-Jones (LJ) particle with a uniaxial quadrupole. We assume that the particles A and B have the quadrupoles with the same magnitude but with the opposite signs. Such a situation can be realized by assuming the same density distribution of charges with the opposite signs for molecules A and B.

II. MODEL AND ITS PROPERTIES

A. Minimal model: uniaxially quadrupolar molecules

Our model molecules are aimed to be a minimal model that can reproduce the LCST-type or the closed-loop phase diagrams. We also expect that a permanent electric dipole is not an essential element for these phase diagrams. Thus, we want to exclude any electric dipole from our model. In order to satisfy these requirements, we introduce model molecules A and B shown in Fig. 2. For the isotropic part of the intermolecular interaction, we assume the usual LJ potential between the same type of molecules (A–A and B–B) [16] and only the repulsive part of the LJ potential between the different types of molecules (A–B) [17], respectively. We assign a common diameter σ and a common interaction strength ϵ to all of these potentials. For the anisotropic part, we assume that each molecule has an electrically polarized rigid rod with a total length $2d$ embedded at the center of the molecule. We assign point charges $\mp 2q$ and $\pm q$ to the center and both ends of the rod in the molecule A/B, respectively. Judging from such charge distributions, the overall net charge (monopole) and all the odd-ordered multipoles (dipole, octupole, ...) of the molecules are vanishing exactly and the quadrupole becomes the leading contribution to the intermolecular Coulomb interaction [18]. Therefore, we can treat the molecule A/B

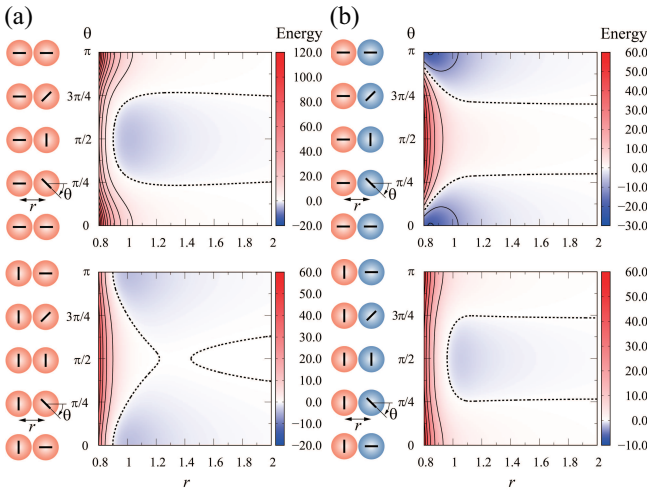

FIG. 3. (Color online) The energy landscapes (a) between the same type of quadrupolar molecules (A–A and B–B) and (b) between different types (A–B). Two variables of the interaction potential are the distance r between the cores of two molecules and the angle θ between two molecular axes embedded in each of the molecules. In the upper panel of each figure, the configuration of molecules is changed from the parallel (colinear) to the perpendicular orientation. On the other hand, in the lower panel, the configuration is changed from the perpendicular to the parallel (non-colinear) one. The magnitude of quadrupole moment is $|Q| = 4.32 \times 10^{-2}$. In all the landscapes, a dashed contour line is drawn along energy zero and the other contour lines are drawn every energy 10.

as a quadrupolar sphere with the quadrupole moment $Q_{\mathrm{A/B}} = \pm 2d^2q$. For the MD simulations, we assign mass m to both ends of the rod in each molecule. Our model molecules are conceptually similar to TIP4P water model [19], which is widely used in the studies on water. The main difference is that TIP4P has electric dipole, while our particles do not. Although the usual LJ particles have only translational degrees of freedom, our model particles shown in Fig. 2 have additional rotational degrees of freedom, which gives a kind of molecular shape to the spherical LJ particle. Due to this reason, we call our simple model particles "molecules." Hereafter, we describe all the physical quantities in non-dimensional units by measuring length, energy, mass, time, and electric charge in the units of σ, ϵ, $2m$, $(2m\sigma^2/\epsilon)^{1/2}$, and the elementary charge e, respectively. In addition, we use reduced temperature by using the unit of ϵ/k_{B}, where k_{B} is the Boltzmann constant.

B. Anisotropic interaction between quadrupolar molecules

Figure 3 is the energy landscapes between the quadrupolar molecules shown in Fig. 2. The energy is comprised of the isotropic part described by the LJ potential and the anisotropic one by the uniaxial quadrupole moment with its magnitude $|Q| = 4.32 \times 10^{-2}$. Two variables of the interaction energy are the distance r between the centers of two molecules and the angle θ between two molecular axes embedded in each of the molecules. The configuration of the two axes at $\theta = 0$ is a parallelly-oriented, *i.e.*, colinear-shaped one in the upper panels of Figs. 3 (a) and (b) and a perpendicularly-oriented, *i.e.*, T-shaped one in the lower panels. From these energy landscapes, we can recognize that there is a clear short-ranged anisotropy in the interaction between two quadrupolar molecules: In the case of a pair of the same species, the T-shaped configuration is more preferred, while in the case of a pair of the different species, the colinear-shaped one is more preferred. Surely, the interaction between a pair of our quadrupolar molecules is anisotropic as with the interaction between a pair of the Stockmayer particles, which consist of a usual LJ particle and a point dipole [20, 21]. However, there are various differences in their behaviors. First, the quadrupole–quadrupole interaction decays with the interparticle distance r as r^{-5} in three dimensional space, while the dipole–dipole interaction decays much more slowly as r^{-3} [22]. This means that the interaction between our quadrupolar particles is a short-ranged interaction, while the interaction between dipolar particles such as Stockmayer particles is a long-ranged one. Next, the quadrupole–quadrupole interaction oscillates more frequently along with the relative orientation between the molecules than the dipole–dipole interaction. In Sec. IV B, we will discuss another different point related to the occurrence of the lower critical point or the closed-loop coexistence region. These differences can surely affect the phase behaviors.

III. SIMULATION METHODS

A. Gibbs ensemble Monte Carlo (GEMC) method

In order to construct a phase diagram of the binary quadrupolar fluid, we perform GEMC simulations [13–15]. Let us consider a system composed of two coupled subsystems as shown schematically in Fig. 4. We take samples from each of the bulk regions of the two coexisting phases, and call them the subsystems I and II. As these subsystems are samples of bulk systems, we can apply the usual periodic boundary conditions to them. In addition, suppose that the temperature, the volume, the pressure, the number of α-type molecules (α = A, B), and their chemical potentials in the subsystem i (i = I, II) are denoted as $T^{(i)}$, $V^{(i)}$, $p^{(i)}$, $N_\alpha^{(i)}$, and $\mu_\alpha^{(i)}$, respectively. In order to realize two-phase equilibrium of the binary system, thermodynamic law requires that the following relations should be satisfied between the two subsystems [1, 23]:

$$T^{(\mathrm{I})} = T^{(\mathrm{II})}, \tag{1}$$

$$p^{(\mathrm{I})} = p^{(\mathrm{II})}, \tag{2}$$

$$\mu_{\mathrm{A}}^{(\mathrm{I})} = \mu_{\mathrm{A}}^{(\mathrm{II})}, \tag{3}$$

$$\mu_{\mathrm{B}}^{(\mathrm{I})} = \mu_{\mathrm{B}}^{(\mathrm{II})}. \tag{4}$$

In usual Monte Carlo simulations including GEMC, we can specify (sub)system temperature as an input parameter. Therefore, when the whole calculation works well, the condition (1) is realized automatically. We should also remember that it is prerequisite that each subsystem is in internal equilibrium. In order to satisfy the internal equilibration and the remaining conditions (2)–(4) in the standard GEMC method, we adopt three types of trial moves shown in Fig. 5. First, local translation and rotation of particles in each subsystem are performed as is shown in Fig. 5 (a). These trial moves ensure the internal equilibration. Next, volume change of the subsystems in Fig. 5 (b) is performed in order to ensure the condition (2). Finally, particle migration from one subsystem to the other one as is shown in Fig. 5 (c) is performed to realize the conditions (3) and (4). Using the GEMC method based on these trial moves, we can achieve the two–phase coexistence without having the interface between different phases. Because the finite size effect of the simulation box mainly comes from the interfacial region with a finite thickness, this GEMC technique can minimize the finite size effect and then miniaturize the simulation box to some extent. The miniaturization of the system size allows us to perform long time simulation runs with which precise determination of the phase

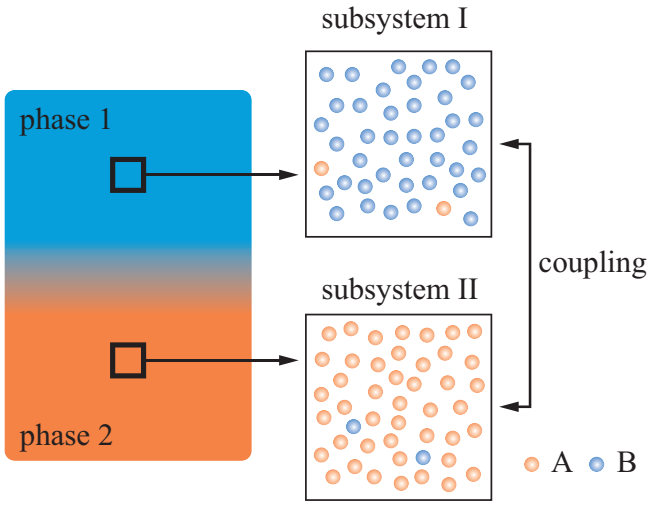

FIG. 4. (Color online) Schematic image of Gibbs ensemble Monte Carlo (GEMC) method. The subsystems I and II are taken from the bulk regions (far from the interface between the two coexisting phases) of the two phases which coexist with each other as sample systems. In GEMC method, the subsystems are coupled and the usual periodic boundary conditions are applied to each of the subsystems.

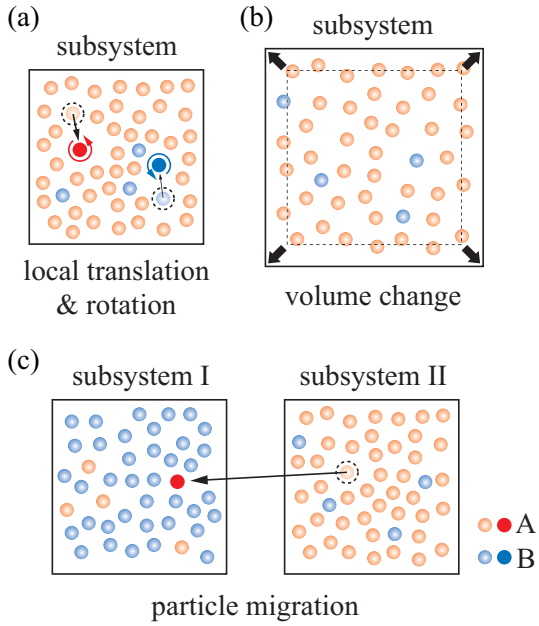

FIG. 5. (Color online) Three trial moves commonly used in the standard GEMC method: (a) local translation and rotation of particles, (b) volume change of the subsystems, and (c) particle migration from one subsystem to the other one. In a condensed system, the trial move (c) becomes practically impossible to be accepted.

diagram can be achieved. In a condensed system, however, the trial particle-insertion procedure shown in Fig. 5 (c) is almost impossible to be accepted. In other words, the trial move leads to the failure in the conditions (3) and (4). This is a serious problem common to Monte Carlo (MC) simulations of the condensed system based on the grand-canonical ensemble. In the next subsection, we will propose a trick to solve this problem.

B. Our simplified scheme of GEMC

In order to improve the difficult situation seen in dense systems discussed in the previous subsection, several efficient algorithms such as the ghost-particle method [24, 25] and the cavity-biased MC method [26] have been devised. Nevertheless, our two-component liquids are too dense (as described in Sec. III D) for these techniques to work well, which tells us that there is a number-density limit above which these methods are no longer effective.

However, there is one case where we can avoid this problem, *i.e.*, the case where the binary system is completely symmetric. In such a case, instead of the particle migration from one subsystem to the other one as a trial move, we can exchange particles A and B between two subsystems, which changes the composition of each subsystem while keeping the total density constant. We set the volumes and the numbers of the molecules in the

subsystems in the following way:

$$V^{(\mathrm{I})} = V^{(\mathrm{II})}, \tag{5}$$

$$N_{\mathrm{A}}^{(\mathrm{I})} + N_{\mathrm{B}}^{(\mathrm{I})} = N_{\mathrm{A}}^{(\mathrm{II})} + N_{\mathrm{B}}^{(\mathrm{II})}, \tag{6}$$

$$N_{\mathrm{A}}^{(\mathrm{I})} + N_{\mathrm{A}}^{(\mathrm{II})} = N_{\mathrm{B}}^{(\mathrm{I})} + N_{\mathrm{B}}^{(\mathrm{II})}. \tag{7}$$

In this case, the following equations are satisfied automatically:

$$\mu_{\mathrm{A}}^{(\mathrm{I})} = \mu_{\mathrm{B}}^{(\mathrm{II})}, \tag{8}$$

$$\mu_{\mathrm{B}}^{(\mathrm{I})} = \mu_{\mathrm{A}}^{(\mathrm{II})}. \tag{9}$$

Instead of the particle migration procedure as shown in Fig. 5 (c), we use an alternative: We exchange the molecule A (B) in one subsystem for the molecule B (A) in the other subsystem [27]. We show a schematic illustration of this trial move in Fig. 6 (b). When the exchange procedure works well, the relation

$$\mu_{\mathrm{A}}^{(\mathrm{I})} - \mu_{\mathrm{B}}^{(\mathrm{I})} = \mu_{\mathrm{A}}^{(\mathrm{II})} - \mu_{\mathrm{B}}^{(\mathrm{II})}. \tag{10}$$

is satisfied in a statistical sense. From Eqs. (8)–(10), we can derive the requirements (3) and (4) for the two-phase equilibrium. As far as the symmetrical system is concerned, the exchange procedure is much more efficient than the particle migration procedure even at very high densities.

For further efficiency, we assume that the whole system composed of the two subsystems obeys the NVT ensemble and that each subsystem obeys the μVT one. In this case, the relations (5)–(7) naturally ensure the condition (2) in an averaged sense, which means that we do not have to try the volume changes of the subsystems as shown in Fig. 5 (b). For the special case of equimolar chemical composition, as a result, the MC procedure can be limited to two kinds of trial moves as shown in Fig. 6: (i) local translation and rotation of a molecule in each subsystem [Fig. 6 (a), which is the same as Fig. 5 (a)] and (ii) exchange of an A–B pair between the two subsystems [Fig. 6 (b)]. In the trial move (i), a randomly selected molecule is given a uniformly random translation within a small cube with each edge length l and a random rotation from $\mathbf{u}$ to $(\mathbf{u}+\gamma\mathbf{v})/|\mathbf{u}+\gamma\mathbf{v}|$. Here, $\mathbf{u}$ is a unit vector parallel to the rigid rod in the molecule before rotation, $\mathbf{v}$ a unit one with a random orientation, and γ a scale factor. In this study, we select the trial moves (i) and (ii) with equal frequency and define $2N$ trial moves as 1 Monte Carlo step (MCS), where N is the total number of molecules in the whole system. This simplified scheme of GEMC is similar to the usage by Das *et al.* [28–30] of semi-grand-canonical Monte Carlo method [15, 31].

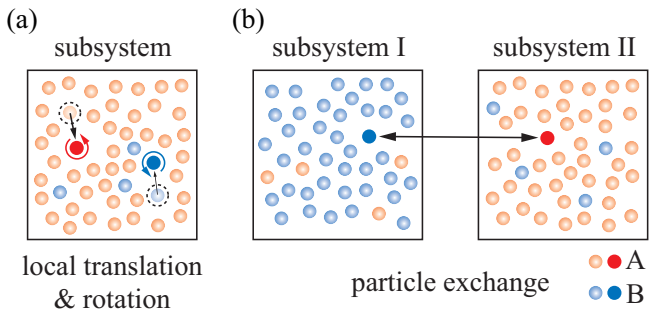

FIG. 6. (Color online) Two trial moves which we adopt in order to promote the equilibration of the system: (a) local translation and rotation of particles and (b) particle identity exchange between the two subsystems. The former move is the same as that in Fig. 5 (a).

C. RATTLE and redistribution of forces on massless points into mass points

After obtaining the closed-loop phase diagram using the GEMC method, we performed MD simulations on the same system with a larger system size. We especially focused on the system in the one-phase regions above the UCST and below the LCST of the closed-loop phase diagram obtained in the GEMC simulation. As described in Sec. II A, our model molecules include a rigid rod, on each end of which a mass m is located (see also Fig. 2). In order to calculate the dynamics of the two-component fluids properly, it is necessary to retain the shape of the rods embedded in the LJ spheres at each time step. Thus, we integrate the equations of motion with the RATTLE algorithm [32, 33], which is a velocity Verlet algorithm with holonomic constraints and their time derivatives. In general case, RATTLE algorithm requires us to solve quadratic and linear simultaneous equations in the update of the positions and velocities of the mass points in the molecules, respectively. For each molecule, we have to solve these simultaneous equations under a set of constraints that are satisfied in terms of Lagrange multipliers. Because of the very simple model molecule of the present study, however, we can solve these set of equations analytically, which reduces the computational cost considerably.

In the following, we explain how to treat the forces acting on massless points in our model molecules. As has been described so far, our spherical molecules have a massless interaction point at their cores. For the correct calculation of MD, we have to redistribute the forces acting on the massless point into the mass points appropriately. Following Berendsen and van Gunsteren [34, 35], we assign half of the forces on the central massless point to each of the two mass points at both ends of the rigid rod inside the molecule, which ensures that both total force and total torque are conserved in each molecule [34].

Throughout this study, we perform MD simulations

with the NVT ensemble. In order to keep the temperature of the system constant, we adopt the Woodcock thermostat [36, 37], *i.e.*, the simple velocity scaling to rescale the velocities of the mass points in the molecules at each time step by a factor of $(T/\mathcal{T})^{1/2}$, where T is the desired temperature and $\mathcal{T}$ is the instantaneous temperature. The heat bath ensures that the distribution of the positions of the mass points at T is canonical.

D. Parameter Setup

Our simulation systems used as the subsystems of the GEMC simulations and as the whole system of the MD simulations are a three-dimensional cubic box with the usual periodic boundary conditions. For the calculation of Coulombic interaction, we perform the Ewald summation [15, 16, 38] with the tabulation method [39] for GEMC and with the particle–particle particle–mesh (P^3M) method [40–43] for MD. We set a dimensionless number $\mathcal{A} = e^2/4\pi\epsilon_0\epsilon\sigma = 6.786 \times 10^2$, where ϵ_0 is the permittivity of vacuum.

Throughout this paper, the following simulation parameters are used. For both of GEMC and MD simulations, the number density of molecules $\rho = 0.8$, the averaged number fraction of molecule A, $x_{\rm A} = 0.5$, and the full length of the rigid rod embedded in the molecule $2d = 0.6$ are used. For the GEMC simulations, we use the total number of molecules $N = 500$ in each subsystem, and for the trial move (i) [Fig. 6 (a)], we set $l = 0.2$ and $\gamma = 0.1$ (see Appendix A for the possibility of artificial anisotropy associated with this trial move). The numbers of steps calculated to average the physical quantities after equilibration at desired temperatures are 10^4 MCSs. About how to equilibrate the systems and how to get the phase coexistence curves in GEMC, readers should refer to Appendix B. For the MD simulations, on the other hand, we use $N = 16,384$ in the whole system and a time increment $\Delta t = 0.005$. The numbers of time steps used to obtain the average physical quantities after equilibration at desired temperatures are 4×10^4 MD steps. For a discussion on the effect of the time increment Δt on the dynamics of the constituent molecules, readers should refer to Appendix D.

IV. RESULTS AND DISCUSSION FOR GEMC SIMULATIONS

A. Phase diagram

Figure 7 is the closed-loop phase diagram (red curve) for the binary system with the magnitude of the quadrupole moment $|Q| = Q_{\rm A} = 4.32 \times 10^{-2}$ ($q = 0.240$) obtained from the GEMC simulations. The phase diagram has two critical points. The critical compositions are both 0.5 and the critical temperatures are estimated as UCST = 4.24 and LCST = 2.16. The familiar critical

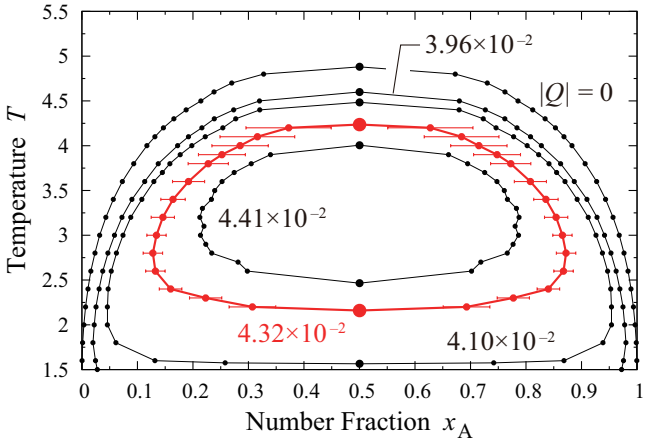

FIG. 7. (Color online) The closed-loop phase diagram for the binary quadrupolar mixture with $|Q| = 4.32 \times 10^{-2}$ (red curve). Two critical temperatures are UCST = 4.24 and LCST = 2.16 (larger red circles). The error bars indicate the standard deviation. For comparison, we show the phase coexistence curves with the other values of $|Q| = 0$, 3.96×10^{-2}, 4.10×10^{-2}, and 4.41×10^{-2} (black curves).

exponents $\beta \simeq 1/3$ for the three-dimensional Ising universality class [44] are observed for both critical points (see Appendix C for details on the critical temperatures and exponents). Similar result has been reported in a previous work [12]. In our simulations, the magnitude of the quadrupole moment $|Q|$ is an important parameter which controls the phase behavior. As is obvious from Fig. 7, the shape of the coexistence region changes from a dome-type shape with one UCST to a closed-loop-type one with both UCST and LCST when the value of $|Q|$ is increased. Further increasing $|Q|$ results in a gradual shrinkage of the closed-loop coexistence region. At a certain critical value of $|Q|$, eventually, the two critical points are expected to merge and to change into a double critical point [4]. This tendency to the polar magnitude is opposite to that of the dome-type gas–liquid coexistence region for one-component Stockmayer fluid [45, 46] and its quadrupolar version, *i.e.*, one-component fluid of LJ particles embedded with a point quadrupole [47].

B. Condition for the occurrence of the lower critical point

In order to understand the phase behavior of our high-density binary quadrupolar mixtures presented in the previous subsection, we perform the angle-averaging of an orientation-dependent interaction between two nearest-neighboring quadrupolar molecules [22]. We note that the angle-averaging of isotropic interactions gives no changes and is meaningless. Generally speaking, in the high temperature limit (or in the nonpolar limit), the Boltzmann factor associated with the quadrupole–

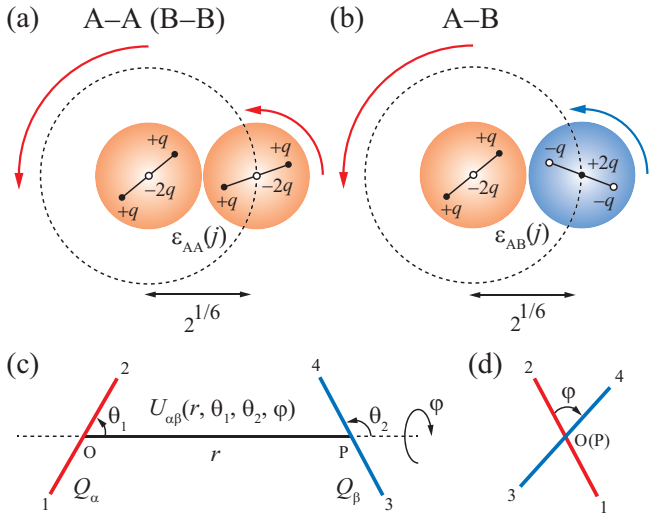

FIG. 8. (Color online) [The upper panel] The microscopic configuration j used for the calculation of the ensemble-averaged energy between our model quadrupolar molecules shown in Fig. 2: (a) a pair of molecules of the same type (A–A and B–B) with the energy $\epsilon_{AA\,(BB)}(j)$ and (b) a pair of molecules of different types (A–B) with $\epsilon_{AB}(j)$. In each case, the centers of the molecules are separated by the distance $2^{1/6}$. [The lower panel] The interaction energy $U_{\alpha\beta}(r, \theta_1, \theta_2, \varphi)$ between pure quadrupoles: (c) the configuration of two interacting uniaxial quadrupoles α and β (α, β = A, B). Here, r is the distance between the centers (O and P) of the quadrupoles and θ_1 and θ_2 are the angles between the axes of the quadrupoles α and β and the line OP, respectively. Numbers 1–4 beside the ends of these axes are just the labels for the identification. (d) A view of the configuration along the line OP. The angle φ means the relative twist of the axes of the quadrupoles about the line.

quadrupole interaction reduces to unity and then the averaged anisotropic interaction in any types of pair becomes exactly zero, which means that there is no anisotropy between any molecules. With a decrease in temperature (or with an increase in the polar magnitude), the contribution to the averaged interaction from the orientations with a negative energy becomes more and more dominant, while that from the orientations with a positive energy approaches zero, which causes the intermolecular anisotropy. The resultant averaged anisotropic energy is always negative, *i.e.*, attractive.

We calculate the angle-averaged interactions between two molecules A and B shown in Fig. 2 based on the method by Fan *et al.* [48]. Their original method was proposed to calculate the effective interaction parameter between two segments for polymeric systems, a low-molecular version of which we will treat in Sec. IV C. Since it is a little complicated, however, we simplify their methodology. Suppose $\epsilon_{\alpha\beta}(j)$ denotes the configurational energy between two neighboring molecules α and β (α, β = A, B) at a microscopic state j. We consider the simplified configurations shown in Figs. 8 (a) and (b): One of two neighboring molecules is fixed at the center of a sphere with a radius $2^{1/6}$; the other molecule is free to move on the spherical surface. The molecular axis of the latter molecule can also be free to rotate. The angle-averaged version of $\epsilon_{\alpha\beta}(j)$ is defined as

$$\langle\epsilon_{\alpha\beta}\rangle = \frac{\mathrm{Tr}\,\epsilon_{\alpha\beta}(j)\,\exp[-\epsilon_{\alpha\beta}(j)/T]}{\mathrm{Tr}\,\exp[-\epsilon_{\alpha\beta}(j)/T]}. \tag{11}$$

A pair of brackets $\langle\cdots\rangle$ means the ensemble average over all the microscopic states. The averaged energy can be decomposed into two parts: $\langle\epsilon_{\alpha\beta}\rangle = \langle\epsilon_{\alpha\beta}\rangle_{\rm i} + \langle\epsilon_{\alpha\beta}\rangle_{\rm a}$. Here, $\langle\epsilon_{\alpha\beta}\rangle_{\rm i}$ is the isotropic part and $\langle\epsilon_{\alpha\beta}\rangle_{\rm a}$ is the anisotopic one. Due to the symmetry between the molecules A and B used in the present study, it is obvious that $\langle\epsilon_{\rm AA}\rangle = \langle\epsilon_{\rm BB}\rangle$. In more detail, $\langle\epsilon_{\rm AA}\rangle_{\rm i} = \langle\epsilon_{\rm BB}\rangle_{\rm i} = -1$, $\langle\epsilon_{\rm AB}\rangle_{\rm i} = 0$, which are independent of temperature, and $\langle\epsilon_{\rm AA}\rangle_{\rm a} = \langle\epsilon_{\rm BB}\rangle_{\rm a}$, which is dependent on temperature. We want to evaluate the values of $\langle\epsilon_{\rm AA}\rangle$ and $\langle\epsilon_{\rm AB}\rangle$ and their anisotopic parts quantitatively. Under the assumption of the configurations as shown in Figs. 8 (a) and (b), we can get the analytical expression of $\langle\epsilon_{\alpha\beta}\rangle$, which includes a little complicated multiple integrals. Thus, we mainly evaluate the integrals with Monte Carlo method [49]. Specifically, we generate $M_{\rm conf}$ pairs of molecular configurations and then we evaluate $\langle\epsilon_{\alpha\beta}\rangle$ approximately using the following expression:

$$\langle\epsilon_{\alpha\beta}\rangle \simeq \frac{\sum_{j}^{M_{\rm conf}} \epsilon_{\alpha\beta}(j)\,\exp[-\epsilon_{\alpha\beta}(j)/T]}{\sum_{j}^{M_{\rm conf}} \exp[-\epsilon_{\alpha\beta}(j)/T]}, \tag{12}$$

where we set $M_{\rm conf} = 5\times10^8$. Once we obtain the approximate values, we can extract their anisotopic parts in the following way: $\langle\epsilon_{\rm AA}\rangle_{\rm a} = \langle\epsilon_{\rm AA}\rangle + 1$ and $\langle\epsilon_{\rm AB}\rangle_{\rm a} = \langle\epsilon_{\rm AB}\rangle$. Figure 9 (a) shows the anisotropic parts of the ensemble-averaged energies between two quadrupolar molecules at several temperatures (T = 1.0, 2.0, 3.0, 4.0, 5.0, and 6.0) as functions of the magnitude of quadrupole moment $|Q|$. We observe that the energy between the different types is more attractive than those between the same type, *i.e.*, $\langle\epsilon_{\rm AB}\rangle_{\rm a} < \langle\epsilon_{\rm AA}\rangle_{\rm a} < 0$, and that the discrepancy is increased with a decrease in temperature or with an increase in the magnitude of the quadrupole moment, which promotes the homogenization of the binary mixtures.

Strictly speaking, as described in Sec. II A, our model molecules are approximately quadrupolar molecules, which means that although the quadrupole is a major contribution to them, they contain to some extent the higher even-ordered multipoles such as hexadecapole. Therefore, we also have to carry out the angle-averaging of a pure quadrupole–quadrupole interaction in order to confirm the validity of the approximation. Figure 8 (c) and (d) are the configuration of two pure uniaxial quadrupoles α and β (α, β = A, B) with quadrupole moments Q_α and Q_β, respectively. Here, r is the distance

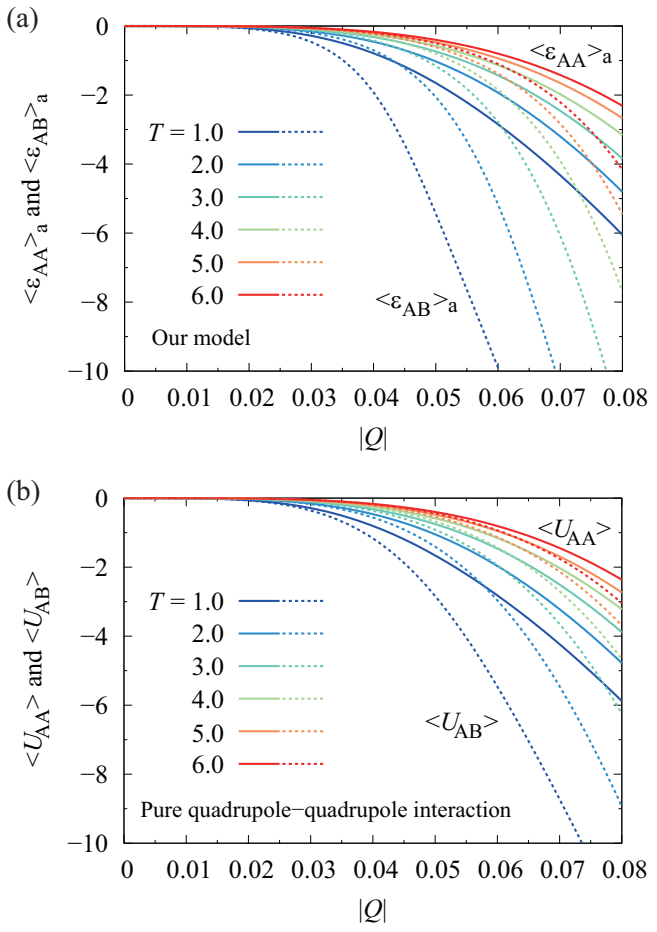

FIG. 9. (Color online) (a) The anisotropic parts $\langle\epsilon_{\alpha\beta}\rangle_{\rm a}$ of the ensemble-averaged energies $\langle\epsilon_{\alpha\beta}\rangle = \langle\epsilon_{\alpha\beta}\rangle_{\rm i} + \langle\epsilon_{\alpha\beta}\rangle_{\rm a}$ between our model quadrupolar molecules α and β (α, β = A, B) and (b) the ensemble-averaged energies $\langle U_{\alpha\beta}\rangle$ between pure quadrupoles α and β. These are functions of the magnitude of quadrupole moment $|Q|$ for different values of temperature T. We set $Q_{\rm A} = -Q_{\rm B} = |Q|$ and fix the distance between the quadrupolar molecules or the quadrupoles at $2^{1/6}$. In both panels, the solid curves correspond to the case of $\alpha = \beta$ (A–A, B–B), while the dashed ones to the case of $\alpha \neq \beta$ (A–B).

between the quadrupolar centers (O and P) and θ_1 and θ_2 are the angles between the axes of the quadrupoles and the line OP. Moreover, the angle φ is that between the two planes formed by the axes with the line OP. The pure quadrupole–quadrupole interaction $U_{\alpha\beta}(r, \theta_1, \theta_2, \varphi)$ corresponding to this configuration is expressed in the following way [22]:

$$U_{\alpha\beta}(r, \theta_1, \theta_2, \varphi) = \frac{3\mathcal{A}Q_\alpha Q_\beta}{4r^5} h(\theta_1, \theta_2, \varphi), \qquad (13)$$

where

$$\begin{aligned} h(\theta_1, \theta_2, \varphi) = {} & 1 - 5\cos^2\theta_1 - 5\cos^2\theta_2 \\ & + 17\cos^2\theta_1\cos^2\theta_2 + 2\sin^2\theta_1\sin^2\theta_2\cos^2\varphi \\ & - 16\sin\theta_1\sin\theta_2\cos\theta_1\cos\theta_2\cos\varphi. \end{aligned} \qquad (14)$$

We can easily derive the angle-averaged version of Eq. (13) as

$$\langle U_{\alpha\beta}\rangle(r) = \frac{\displaystyle\int {\rm d}\Omega\, U_{\alpha\beta} \exp\left[-\frac{U_{\alpha\beta}}{T}\right]}{\displaystyle\int {\rm d}\Omega \exp\left[-\frac{U_{\alpha\beta}}{T}\right]}, \qquad (15)$$

where ${\rm d}\Omega = \sin\theta_1 \sin\theta_2\, {\rm d}\theta_1 {\rm d}\theta_2 {\rm d}\varphi$ and the integrals are taken over $\theta_1 = 0 \sim \pi$, $\theta_2 = 0 \sim \pi$, and $\varphi = 0 \sim 2\pi$. After setting $Q_{\rm A} = -Q_{\rm B} = |Q|$ and $r = 2^{1/6}$, we evaluate the integrals included in Eq. (15) numerically, not with Monte Carlo method. We show the ensemble-averaged energies $\langle U_{\alpha\beta}\rangle$ between two pure quadrupoles at several temperatures as functions of the magnitude of quadrupole moment $|Q|$ in Fig. 9 (b). Obviously, the behavior of $\langle U_{\alpha\beta}\rangle$ is qualitatively the same as that of $\langle\epsilon_{\alpha\beta}\rangle_{\rm a}$, which ensures that our model molecules can be actually regarded as quadrupolar molecules and that the discussion in the present study is based on the quadrupole–quadrupole interaction.

Subsequently, we discuss a condition for the occurrence of the lower critical point or the closed-loop coexistence region in more details. When the quadrupole moments of two types of molecules A and B have the same sign ($Q_{\rm A} \cdot Q_{\rm B} > 0$), of course, either of the averaged energies between the same type of molecules (A–A and B–B) is more attractive than that between the different types of molecules (A–B). In the special case of the same magnitude ($Q_{\rm A} = Q_{\rm B}$), all the averaged energies are exactly consistent. Conversely, when the quadrupole moments have the opposite signs ($Q_{\rm A} \cdot Q_{\rm B} < 0$) and comparable magnitudes, the energy between the different types is more attractive than those between the same type as shown in Fig. 9 (a). The stronger attraction between different species, together with the entropy of mixing, drives the mixing of the two components against the isotropic attraction between similar species. The mixing tendency is amplified with decreasing temperature or with increasing the magnitude of the quadrupole moments and then enhanced to the maximum for the symmetric system as with our model ($Q_{\rm A} = -Q_{\rm B}$), which results in the occurrence of the closed-loop coexistence region and its shrinkage. In order to explain the mechanism of the phase behavior of the one-component dipolar or quadrupolar fluid with the gas–liquid coexistence region, on the other hand, we can use the Flory–Huggins description for ordinary polymer solutions [45, 46]. The description predicts that the longer the polymer chain are, the more upward the UCST shifts. In the one-component polar fluids, an increase in the magnitude of the dipole or quadrupole moment enhances the growth of the aggregates composed of the same type of molecules. Such an upward shift of UCST is the result of the growth of the molecular aggregates.

C. Comparison with the lattice model of binary solutions

In order to check the validity of the closed-loop coexistence region for our binary fluid, we calculate a dimensionless effective interaction parameter between two nearest-neighboring molecules A and B. The quantity is called the χ parameter in the Flory–Huggins model for polymer solutions. We have to modify the parameter to fit our binary quadrupolar fluid. Using the averaged energies $\langle\epsilon_{\alpha\beta}\rangle$ introduced in Sec. IV B, we express the modified parameter $\chi_{\rm eff}(T)$ in the following way:

$$\chi_{\rm eff}(T) = \frac{z}{T}\Big[\langle\epsilon_{\rm AB}\rangle - \frac{1}{2}(\langle\epsilon_{\rm AA}\rangle + \langle\epsilon_{\rm BB}\rangle)\Big], \tag{16}$$

where z is the coordination number of the nearest-neighboring pairs. We consider the number z as a constant, which is a reasonable assumption in constant volume simulations of the condensed system like the fluids used in this study. As discussed in Sec. IV B, the symmetry between the molecules A and B enables us to rewrite Eq. (16) into

$$\chi_{\rm eff}(T) = \frac{z}{T}\Big[\langle\epsilon_{\rm AB}\rangle_{\rm a} - \langle\epsilon_{\rm AA}\rangle_{\rm a} + 1\Big]. \tag{17}$$

In the special case when $\epsilon_{\alpha\beta}(j)$ is completely isotropic, *i.e.*, $\langle\epsilon_{\rm AA}\rangle_{\rm a} = \langle\epsilon_{\rm AB}\rangle_{\rm a} = 0$, $\chi_{\rm eff}(T)$ reduces to the original χ parameter. The binary fluids with $|Q| = 0$ treated in the present study are an example of this case. In addition, $\chi_{\rm eff}(T)$ usually indicates a variety of temperature dependence, while the original $\chi(T)$ shows a simple behavior due to the form $\chi(T) = \mathcal{C}/T$, where $\mathcal{C}$ is generally

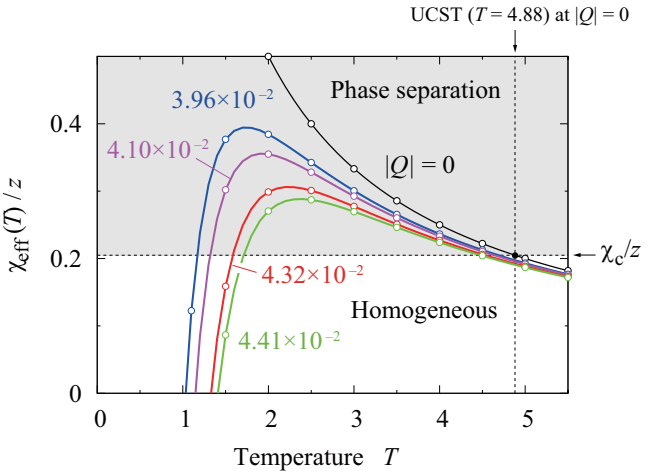

FIG. 10. (Color online) The effective interaction parameters $\chi_{\rm eff}(T)$ as functions of temperature T for different values of $|Q|$. The open circles show the results from direct numerical integration of Eq. (11); the solid curves show the results from numerical integration using Monte Carlo method. When the effective interaction parameter is in the gray region, the system undergoes a liquid–liquid phase separation.

a positive constant. Figure 10 shows the temperature dependence of $\chi_{\rm eff}(T)/z$ for the system with several magnitudes of quadrupole moment ($|Q| = 0$, 3.96×10^{-2}, 4.10×10^{-2}, 4.32×10^{-2}, and 4.41×10^{-2}). Without loss of generality, the parameter $\chi_{\rm eff}(T)$ is a useful criterion for the liquid–liquid phase separation [23, 50, 51]: When the parameter is larger than a critical value $\chi_{\rm c}$ ($\chi_{\rm eff}(T) > \chi_{\rm c}$), the system causes the phase separation. Inversely, when $\chi_{\rm eff}(T) < \chi_{\rm c}$, the system keeps a spatially homogeneous one-phase state. In the present study, we define $\chi_{\rm eff}(T)/z \simeq 0.2$ at UCST $= 4.88$ of the system with $|Q| = 0$ as the common threshold $\chi_{\rm c}/z$ (see also Table II in Appendix C). In Fig. 10, we find that the systems with the finite moment ($|Q| \neq 0$) exceed the critical value $\chi_{\rm c}$ and then fall below it again with increasing temperature. This is a reasonable proof for the occurrence of a closed-loop coexistence region. For condensed binary mixtures of dipolar particles such as Stockmayer particles, on the other hand, we have confirmed that the corresponding effective parameter $\chi_{\rm eff}(T)$ takes not such turnover profiles but monotonic decay ones similar to the curve for the system with $|Q| = 0$ in Fig. 10. To the best of our knowledge, actually, computational and theoretical studies on two-component dipolar mixtures have never observed the occurrence of the lower critical point or the closed-loop coexistence region [52, 53].

Next, we calculate the phase diagrams for our condensed binary quadrupolar fluids based on a lattice theory of solutions and then compare them with those obtained by GEMC simulations (Fig. 7). Let us consider a binary mixture composed of two small molecules A and B with the same size and with respective number fractions $x_{\rm A}$ and $x_{\rm B} = 1 - x_{\rm A}$. In addition, we describe the whole system with a set of lattice cells with the same size as the molecules and assume that each cell is occupied by only one molecule under the incompressibility condition of the system. When the binary system is mixed homogeneously, the free energy of mixing per lattice site is expressed as the form of $f(x_{\rm A})\,T$ and $f(x_{\rm A})$ is given in the following way [23, 50]:

$$\begin{aligned} f(x_{\rm A}) = {} & x_{\rm A}\ln x_{\rm A} + (1 - x_{\rm A})\ln(1 - x_{\rm A}) \\ & + \chi_{\rm eff}(T)\, x_{\rm A}(1 - x_{\rm A}). \end{aligned} \tag{18}$$

We should note that the original lattice model of solutions was proposed for the condensed mixtures dominated by the van der Waals interactions. In this case, $\chi_{\rm eff}(T)$ in Eq. (18) is replaced with the original χ parameter with the form of $\chi(T) = \mathcal{C}/T$ as described above. The symmetry of the system enables us to use the simple phase equilibrium condition for determining the coexistence curve, *i.e.*, the binodal curve:

$$\frac{\partial f(x_{\rm A})}{\partial x_{\rm A}} = 0. \tag{19}$$

Subsequently, the spinodal condition for determining the spinodal line is given by

$$\frac{\partial^2 f(x_{\rm A})}{\partial x_{\rm A}^2} = 0 \tag{20}$$

and then the critical points ($x_{\mathrm{A,c}}$, $\chi_{\mathrm{eff}}(T_{\mathrm{c}})$) can be obtained as the solutions of the following simultaneous equations:

$$\frac{\partial^2 f(x_{\mathrm{A}})}{\partial x_{\mathrm{A}}^2} = 0, \tag{21}$$

$$\frac{\partial^3 f(x_{\mathrm{A}})}{\partial x_{\mathrm{A}}^3} = 0. \tag{22}$$

Although Eqs. (19) and (20) have to be solved numerically, the simultaneous Eqs. (21) and (22) can easily be solved analytically, which gives the following solutions:

$$x_{\mathrm{A,c}} = \frac{1}{2}, \tag{23}$$

$$\chi_{\mathrm{eff}}(T_{\mathrm{c}}) = 2. \tag{24}$$

By substituting $T_{\mathrm{c}} = 4.88$ (UCST) and $\langle \epsilon_{\alpha\beta} \rangle_{\mathrm{a}} = 0$ of the system with $|Q| = 0$ into Eqs. (17) and (24), we determine the coordination number $z = 2T_{\mathrm{c}} = 9.76$ approximately. Figure 11 (a) is the binodal curves for our binary fluids with several magnitudes of quadrupole moment ($|Q| = 0$, 3.96×10^{-2}, 4.10×10^{-2}, 4.32×10^{-2}, and 4.41×10^{-2}), which are calculated numerically based on the lattice model of binary solutions. Each curve corresponds to the curve $\chi_{\mathrm{eff}}(T)/z$ with the same color as in Fig. 10. Clearly, the binary fluids with the finite moment ($|Q| \neq 0$) reproduce the closed-loop coexistence region, as expected from the temperature dependence of $\chi_{\mathrm{eff}}(T)/z$ shown in Fig. 10. Moreover, the closed-loop coexistence region shrinks monotonically with an increase in $|Q|$. These behaviors of the phase diagrams obtained from the lattice model are qualitatively the same as those from the GEMC simulations (see Fig. 7) except that the mean-field model for the binary fluids with $|Q| = 3.96 \times 10^{-2}$ reproduces the closed coexistence curve, while the GEMC simulations for the corresponding system does not in the temperature range ($T \geq 1.5$) we have calculated in the present study. If we perform more GEMC simulations for the system in the temperature region lower than $T = 1.5$, the dome-type coexistence curve may close. In order to compare the result of the mean-field model with that of the GEMC simulations in more detail, we show both closed binodal curves for the system with $|Q| = 4.32 \times 10^{-2}$ in Fig. 11 (b). The gray area painted in Fig. 11 (b) is a thermodynamically unstable region, where the system causes spontaneous phase separation known as spinodal decomposition [54], and its boundary shown by the dashed line is the spinodal line. There are two significant differences between the two closed curves due to the different methods: (i) Both upper and lower critical points in GEMC belong to the three-dimensional Ising universality class ($\beta \simeq 1/3$), while those in the lattice model of solutions to the usual mean-field universality class ($\beta = 1/2$). (ii) The two-phase coexistence region in GEMC is smaller than that in the mean-field model. We conclude that these differences mainly come from the correlation between the constituent molecules and the thermal fluctuation in the whole system and that the appearance of the closed-loop immiscible region itself is independent of the above correlation and fluctuation and mainly determined by the

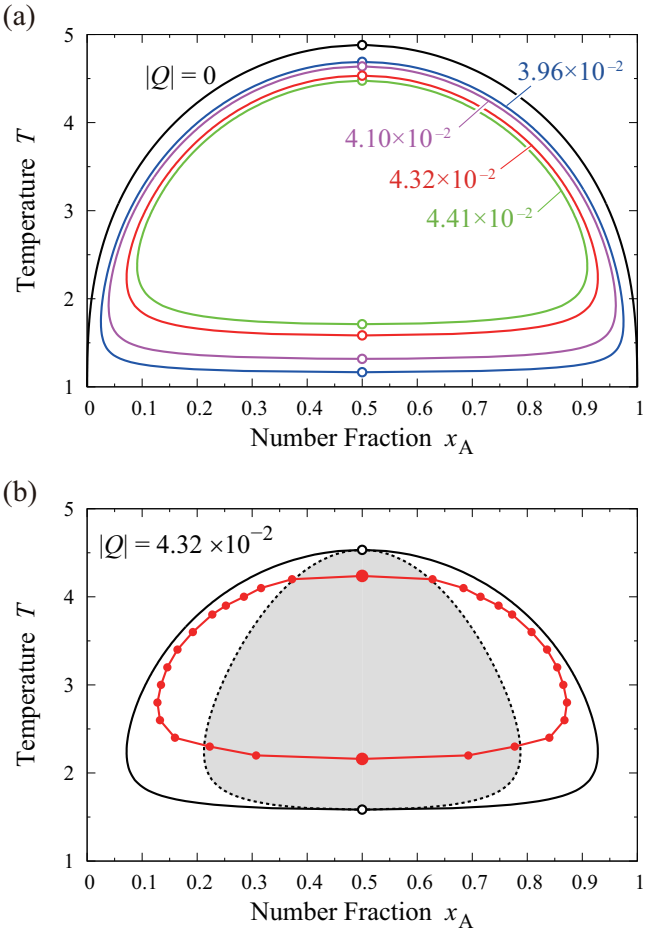

FIG. 11. (Color online) (a) Phase diagrams of our binary quadrupolar mixtures calculated with the lattice model of solutions, where the effective parameter $\chi_{\mathrm{eff}}(T)$ shown in Fig. 10 is applied to the free energy of mixing, Eq. (18). Solid curves are the phase coexistence curves, *i.e.*, binodal curves, for different values of $|Q|$ and the critical points are indicated by the open circles on the curves. (b) Comparison of the phase diagram of the binary mixtures with $|Q| = 4.32 \times 10^{-2}$ obtained from GEMC simulations (Fig. 7) with that of the identical system calculated with the lattice model. The binodal curve from the GEMC simulations is drawn with the red line. On the other hand, the binodal and the spinodal curves from the lattice model are drawn with the black solid and dashed curves, respectively. In the gray area inside the dashed curve, the system is thermodynamically unstable. The coordination number z is assumed to be independent of $|Q|$ and determined from the critical relation $\chi_{\mathrm{c}} = z/T_{\mathrm{c}} = 2$ for the binary LJ fluids with $|Q| = 0$, where $T_{\mathrm{c}} = 4.88$ (see also Table II in Appendix C).

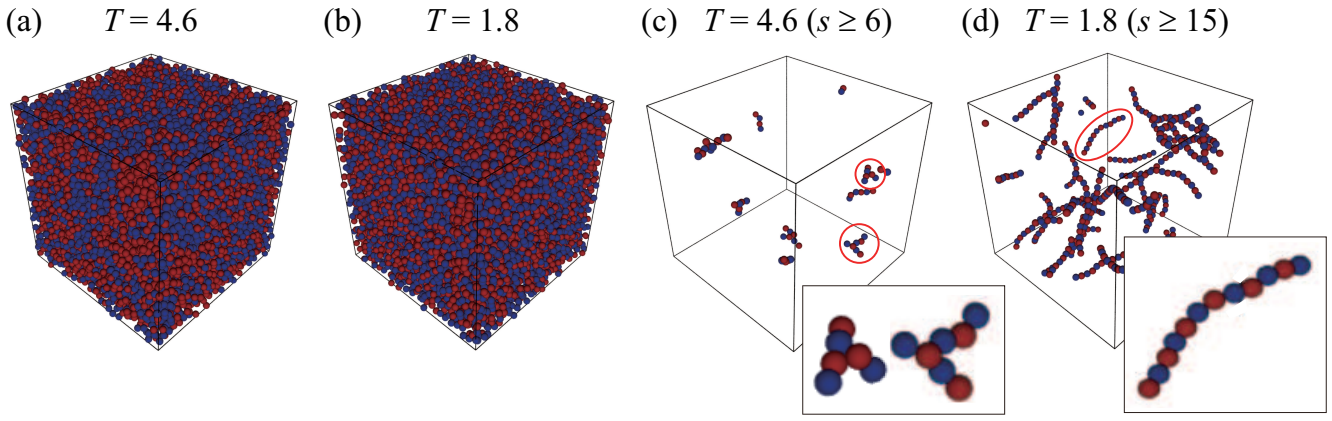

FIG. 12. (Color online) Snapshots of the MD simulations for the binary system with $|Q| = 4.32 \times 10^{-2}$, $N = 16,384$, and $x_A = 0.5$. Red and blue particles correspond to molecules A and B, respectively. Full images at two different homogeneous phases: (a) $T = 4.6$ (above the red curve in Fig. 7) and (b) $T = 1.8$ (below). Aggregates with the sizes of (c) $s \geq 6$ and (d) $s \geq 15$ extracted from (a) and (b), respectively. In (c) and (d), characteristic aggregates in each case are marked by red open circles, whose enlarged pictures are shown in the insets.

magnitude of the quadrupole moment $|Q|$ as discussed in Sec. IV B.

V. RESULTS AND DISCUSSION FOR MD SIMULATIONS

In the previous section, the GEMC calculations of a relatively small system size and the mean-field lattice model on our binary quadrupolar mixtures showed us that the occurrence of the closed-loop phase coexistence region in the binary fluids is not artificial but physically meaningful. However, we cannot get sufficient information about the microscopic structures existing in the binary fluids through these approaches. In order to investigate these microscopic structures, we performed MD simulations of a larger system size. In this section, we discuss the results obtained from the MD simulations.

A. Structural properties

Figures 12 (a) and (b) are typical snapshots of the binary system with $|Q| = 4.32 \times 10^{-2}$, $N = 16,384$, and $x_A = 0.5$ at $T = 4.6$ and 1.8 (outside the closed red curve in Fig. 7), respectively. They are in a stable homogeneous phase and there are no differences in appearance, although they are appreciably different in the magnitude of the thermal fluctuation. In order to discuss structural properties in the stable one-phase region in more details, we define the short-ranged anisotropic bond between different types of molecules: When the distance between a pair of charges of different signs belonging to different types of molecules is shorter than 0.60, we regard that the anisotropic bond between these two charges is formed. The threshold value is determined from the radial distribution function at $T = 1.5$ (see Appendix E for details). Now, we can define aggregates connected by the anisotropic bonds. Let us denote the size of the aggregate (the number of constituent molecules) by s. Figures 12 (c) and (d) are characteristic aggregates with more than a certain size [(c) $s \geq 6$ and (d) $s \geq 15$] observed in Figs. 12 (a) and (b), respectively. The former aggregates have flexible structures with branch points, while the latter have semiflexible linear string-like structures with random orientations. In both cases, the aggregates are composed of alternating arrays of the two types of molecules. We can qualitatively understand the preferred shape of the aggregates in the stable one-phase region by considering the rotational free energy of a pair of nearest-neighboring molecules with the quadrupoles of the opposite signs. The energy landscape in the upper panel of Fig. 3 (b) shows that the linear string-like aggregates are stabilized by the strong orientation between the axes in the adjacent molecules. On the other hand, the branched aggregates have the bonding energy e_b and entropy s_b larger than the string-like ones ($\Delta e_b > 0$ and $\Delta s_b > 0$). Thus, the rotational free energy change $\Delta f_b = \Delta e_b - T\Delta s_b$ tells us that linear string-like aggregates are preferred more at low temperatures, while branched one at high temperatures, which is consistent with the shapes of the aggregates in Figs. 12 (c) and (d).

B. Cluster size distributions

Figure 13 shows the size distributions n_s of the aggregates existing in the equimolar binary system with $|Q| = 4.32 \times 10^{-2}$ and $N = 16,384$ at several temperatures below LCST and above UCST. Each distribution

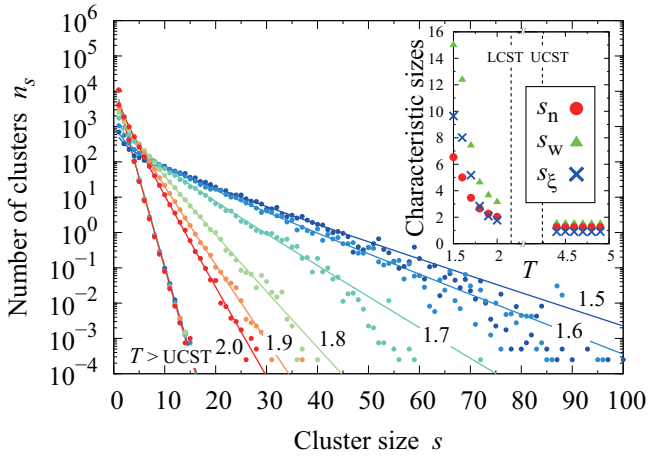

FIG. 13. (Color online) Size distributions n_s of the aggregates existing in the equimolar binary system with $|Q| = 4.32\times10^{-2}$ and $N = 16,384$. As the temperature changes from $T = 1.5$ to 2.0 ($<$ LCST), the distribution changes from blue points to red ones. On the other hand, the size distributions at temperatures $T = 4.4$ to 4.9 ($>$ UCST) are almost overlapped. These data are plotted in semilogarithmic scales. The inset shows three characteristic aggregate sizes, s_n, s_w, and s_ξ, as functions of temperature.

can be fitted with a function

$$f(s) = A\, s^{-\tau} \exp\left[-\frac{s}{s_\xi}\right], \tag{25}$$

where A is a coefficient, τ is a critical exponent, which is known as Fisher exponent, and s_ξ is a characteristic aggregate size [55]. We obtain $\tau = 0.44$ from the optimization with the system at $T = 1.5$ and then adjust the other parameters A and s_ξ according to each temperature. We observe that the distributions below LCST are sensitive to temperature, while those above UCST are almost independent of the temperature. The inset of Fig. 13 shows the temperature dependence of three characteristic aggregate sizes: the number-averaged aggregate size s_n, the weight-averaged one s_w, and s_ξ. The former two quantities are defined in the following way [50, 51]:

$$s_n = \sum_{s=1}^{N} s\, n_s \Big/ \sum_{s=1}^{N} n_s, \tag{26}$$

$$s_w = \sum_{s=1}^{N} s^2\, n_s \Big/ \sum_{s=1}^{N} s\, n_s, \tag{27}$$

where the relation $s_w \geq s_n$ is always satisfied. In the inset, we cannot observe a sign of divergence of the characteristic sizes at the two critical points, where the correlation lengths of the thermal fluctuation of the composition diverge [44, 54]. Therefore, there are no tricritical points in our binary quadrupolar fluid, where the thermodynamic critical point and the percolation transition point are overlapped [51, 56]. Judging from the temperature dependence of three characteristic aggregate sizes in the inset, we expect that the percolation transition point should exist in the temperature region lower than $T = 1.5$, if it exists. Here, we should notice that the transition is not the real sol–gel transition, because the aggregates below LCST are mainly linear and do not have branch points, which are essential elements in the gel (the network). Since we can regard the characteristic size s_ξ of the aggregates as a kind of correlation length [55], the monotonic increase of s_ξ with decreasing temperature indicates an increase in the extent of the correlation between the molecular clusters. Similarly, the cage-like structures of water formed with hydrogen bonds, *i.e.*, the components of the hydrogen bond network in water, become closely correlated with each other with a decrease in temperature [57]. Hence, we conclude that the common correlation behavior between the molecular clusters observed in water and our binary fluid is one of the general properties of the anisotropic interactions including the hydrogen bonding.

VI. SUMMARY AND OUTLOOK

We have clarified several macroscopic and microscopic properties of the binary quadrupolar fluid using molecular simulations. Main results are as follows:

(i) The binary mixture of the molecules with the quadrupoles of the same (or comparable) magnitude but of the opposite signs can possess a closed-loop immiscible region. The closed-loop coexistence region shrinks gradually with an increase in the magnitude of the quadrupole moment. On the other hand, the dipole–dipole interaction does not cause the closed-loop coexistence region, irrespective of the strength of the dipole moment. To the best of our knowledge, this is the first study to discuss a condition for the occurrence of the lower critical point or the closed-loop coexistence region in the binary mixtures in detail from the point of view of multipole–multipole interaction between the constituent molecules.

(ii) In terms of critical phenomena, there is no difference between the upper critical point and the lower critical one. Both critical points belong to the three-dimensional Ising universality class regardless of the magnitude of quadrupole moment, *i.e.*, the strength of the anisotropic interaction due to the quadrupoles.

(iii) In spatially homogeneous phases above and below the closed coexistence curve, the aggregates composed of alternating arrays of the two types of molecules are formed. The shape of the aggregates are sensitive to the level of the thermal fluctuation: The aggregates above UCST are flexible and

branched, while those below LCST are semiflexible and linear.

(iv) The size distributions of the aggregates in the equimolar binary fluid at several temperatures outside the closed coexistence region are exponential in size. The distributions below LCST are sensitive to temperature, while those above UCST are almost the same regardless of temperature. In addition, the characteristic sizes of the aggregates do not diverge at the upper and lower critical points, where the characteristic sizes of the thermal fluctuation of the composition diverge. The behavior indicates that our binary quadrupolar fluids do not have no tricritical points.

The quadrupolar model molecule that we have proposed in this paper should be a minimal model which can reproduce the closed-loop phase diagram in the binary system. Fortunately, our model molecule is free from the artifact of the discreteness in spatial arrangement and interaction that the usual lattice models possess. From the computational point of view, the molecule is also easy to treat. Hence, we expect that the binary quadrupolar fluids can be a useful starting point to study closed-loop phase diagrams. For example, it is very interesting to examine the binary mixtures under an external flow. When a shear flow is imposed on such a system, the closed coexistence region will probably be shifted (or may disappear or appear newly), which is known as shear-induced phase transitions [58, 59]. In our future publications, we will examine both structural and rheological properties of the binary quadrupolar mixtures under external flow by the nonequilibrium molecular dynamics (NEMD) simulations [60].

ACKNOWLEDGMENTS

MT would like to thank Prof. T. Indei, Dr. T. Nakamura, Dr. M. Yoneya, Dr. H. Morita, Dr. T. Uneyama, and Prof. T. Koga for valuable comments. This research was financially supported by CREST, JST.

Appendix A: Possibility of anisotropy involved with the local translation of molecules in GEMC

As explained in the main text, we set the length of each edge of a small cube used for the trial translational move of the molecules [Fig. 6 (a)] to $l = 0.2$. Since the mean distance between the nearest-neighboring molecules in each subsystem (~ 1) is larger than the standard deviation of the trial translational move of the molecules (0.1), the artifact due to the anisotropy of the small cube may be worried. Actually, however, the detailed-balance condition for the trial moves is maintained and the radial distribution functions obtained from GEMC calculations are quantitatively consistent with those obtained from MD calculations (see also Appendix E). Therefore, there is no problem.

Appendix B: Equilibration of the system in GEMC and the liquid–liquid equilibrium data

Figure 14 is the convergence of the states at several temperatures of a binary mixture with $|Q| = 4.32 \times 10^{-2}$ in the GEMC simulations. We use the exchange procedure explained in Sec. III B. For the temperatures simulated in this work, the compositions in the subsystems I and II reach an equilibrium value immediately after the temperature is set to a desired value at 0 MCS as shown in Figs. 14 (a)–(e). Due to this quick convergence, the system can reach the equilibrium state within 10^4 MCSs. Thus, we use the data in the range of 10^4–2×10^4 MCSs to calculate the equilibrium quantities.

Here, we explain how to sample the number fractions of the molecule A in the two subsystems [15]. First, when both subsystems have almost the same number fraction as shown in Figs. 14 (a) and (e), in principle, we can treat the data obtained from GEMC as the same as those from the usual NVT ensemble Monte Carlo simulations. Next, when the subsystems always correspond to either of two coexisting phases as shown in Figs. 14 (b) and (c), we can average the number fraction in each subsystem separately to obtain the averaged number fraction of the molecule A in each phase. Finally, when the number fractions exchange frequently between the two subsystems as shown in Fig. 14 (d), we construct a histogram of the probability density $P(x_{\mathrm{A}})$ from the time sequence of the number fractions in the two subsystems. In this case, the histogram has a symmetric double peak structure and can be fitted well by the sum of two Gaussian functions:

$$P(x_{\mathrm{A}}) = a \exp\left[-\frac{(x_{\mathrm{A}} - 0.5 + c)^2}{b}\right] + a \exp\left[-\frac{(x_{\mathrm{A}} - 0.5 - c)^2}{b}\right], \tag{B1}$$

where a, b, and c are a set of positive parameters. Once we get the parameters through the fitting procedure, we also obtain the number fractions of the molecule A at equilibrium state as $x_{\mathrm{A,\,I}} = 0.5 - c$ and $x_{\mathrm{A,\,II}} = 0.5 + c$ ($x_{\mathrm{A,\,I}} < x_{\mathrm{A,\,II}}$). Here, $x_{\mathrm{A},\,i}$ (i = I, II) is the number fraction of the molecule A in the subsystem i. In Table I, we present the liquid–liquid equilibrium data ($x_{\mathrm{A,\,I}}$, T) of the binary quadrupolar fluids at several magnitudes of quadrupole moment obtained in the manner described above.

Appendix C: Approximate estimate of a critical exponent and critical temperatures

In this appendix, we explain how to determine a critical exponent and critical temperatures for our binary

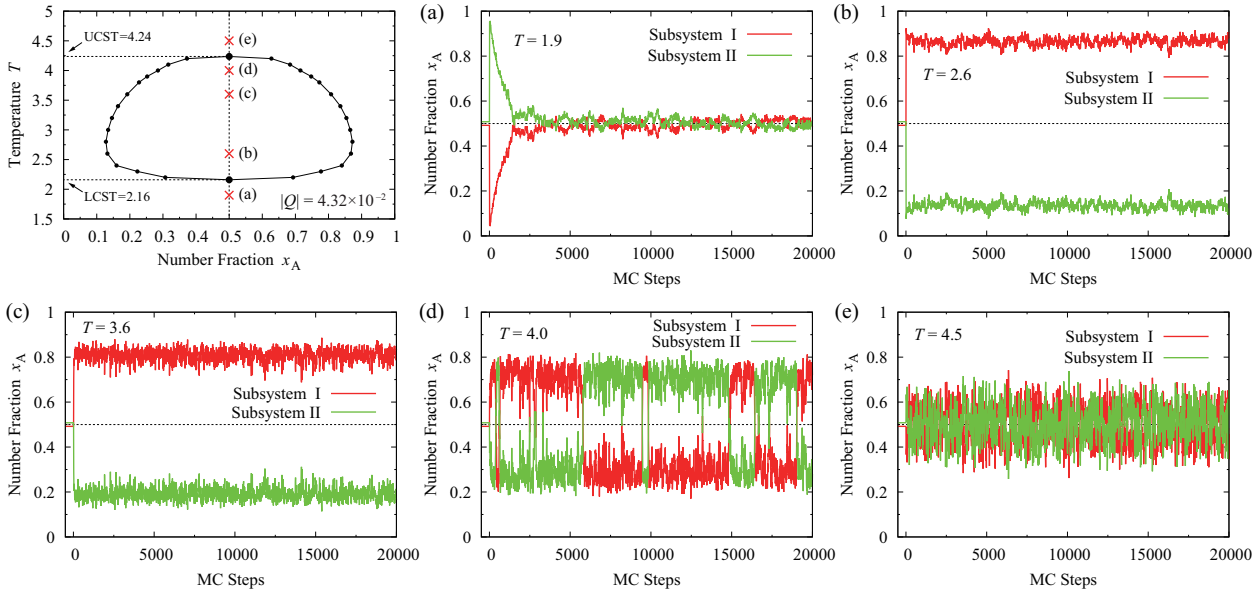

FIG. 14. (Color online) GEMC convergence of several states on the closed-loop phase diagram for the binary system with $|Q| = 4.32 \times 10^{-2}$ and $N = 16,384$. The composition is equimolar ($x_{\rm A} = 0.5$) and the temperature is as follows: (a) $T = 1.9$, (b) 2.6, (c) 3.6, (d) 4.0, and (e) 4.5. The correspondence between a pair of parameters ($x_{\rm A}$, T) and the state is indicated with the red cross marks on the phase diagram in the upper left. In each state, the temperature is set a desired value at 0 MCS and then we perform GEMC calculation during 2×10^4 MCSs. In (a)–(e), the red line means the number fraction $x_{\rm A,\,I}$ of molecule A in the subsystem I and the green one the number fraction $x_{\rm A,\,II}$ in the subsystem II.

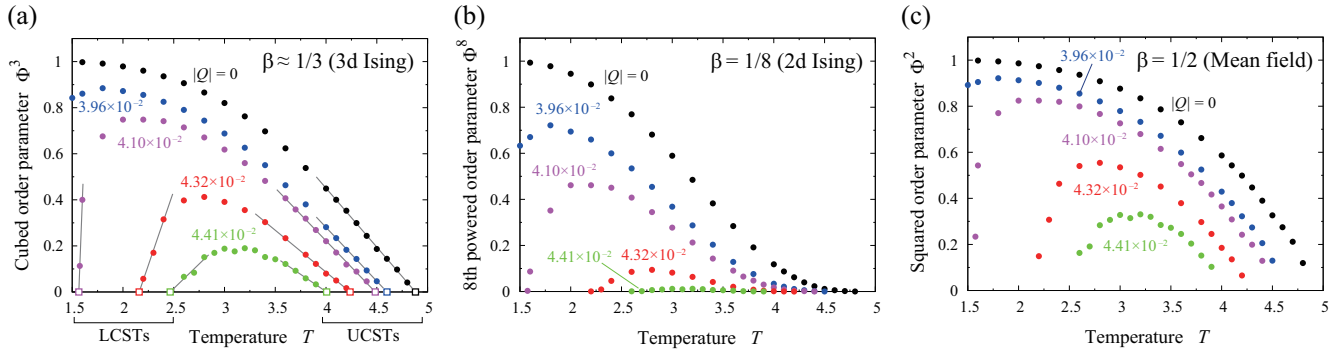

FIG. 15. (Color online) The $1/\beta$-th power of the order parameter $\Phi^{1/\beta}$ as a function of temperature. The order parameter is defined as $\Phi \equiv x_{\rm A,\,II} - x_{\rm A,\,I}$. (a) $\beta = 1/3$ (3d Ising universality class), (b) 1/8 (2d Ising), and (c) 1/2 (mean field theory). In (a), extrapolated critical temperatures are shown by open squares.

quadrupolar mixtures. For these purposes, we introduce an order parameter defined as $\Phi \equiv x_{\rm A,\,II} - x_{\rm A,\,I}$. The theory of critical phenomena tells us that the order parameter near the critical temperature $T_{\rm c}$ shows the following behavior [44]:

$$\Phi = B|T - T_{\rm c}|^{\beta}, \tag{C1}$$

where B is a numerical coefficient and β is a critical exponent. In binary symmetric mixtures, of course, the critical number fraction $x_{\rm A,\,c}$ is exactly 0.5. The relation (C1) is satisfied in the region of $T < T_{\rm c}$ when $T_{\rm c}$ = UCST and in the region of $T > T_{\rm c}$ when $T_{\rm c}$ = LCST. This also means that the $1/\beta$-th power of the order parameter, *i.e.*, $\Phi^{1/\beta}$, changes linearly with temperature around the critical point, when the exponent β is chosen correctly. We show $\Phi^{1/\beta}$ as a function of temperature in Fig. 15, where (a) $\beta = 1/3$ (corresponding to 3d Ising universality class), (b) $\beta = 1/8$ (2d Ising), and (c) $\beta = 1/2$ (mean field theory). In Fig. 15 (a), the parameter Φ^3 ($\beta = 1/3$) approaches zero linearly around $\Phi^3 \simeq 0$ as is expected from the critical behavior. On the other hand, (b) Φ^8 ($\beta = 1/8$) and (c) Φ^2 ($\beta = 1/2$) do not show linear decrease to zero. As a result, the value $\beta = 1/3$ is closest to the critical exponent for our binary mix-

tures, with which we conclude that our system belongs to the three-dimensional Ising universality class regardless of the magnitude of quadrupole moment. Furthermore, we can determine the critical temperatures by a linear extrapolation of Φ^3 to zero. Table II shows the estimated critical temperatures of the binary quadrupolar fluids.

Appendix D: The effect of the time mesh width Δt on the dynamics of the molecules

In order to solve the equations of motion for the quadrupolar molecules, we use the time mesh width $\Delta t = 0.005$. It is necessary to check whether this time mesh width is sufficiently small for the translational dynamics of the molecular centers as well as the rotational dynamics of the molecular axes. For this purpose, we calculated the mean-squared displacement $\langle|\mathbf{r}(t) - \mathbf{r}(0)|^2\rangle$ and the time-dependent orientational correlation function $\langle \mathbf{u}(t) \cdot \mathbf{u}(0)\rangle$ as functions of time t. Here, $\mathbf{r}(t)$ is the position of the molecular center and $\mathbf{u}(t)$ is the director, *i.e.*, the normalized vector parallel to the molecular axis embedded in the molecule. A pair of brackets $\langle \cdots \rangle$ means the ensemble average for all the molecules A or B.

When the translational motions of the molecular centers are described by the mutually uncorrelated Brownian dynamics, we can get a simple expression for the mean-squared displacement at long times [61]:

$$\langle|\mathbf{r}(t) - \mathbf{r}(0)|^2\rangle = 2d_{\rm s}Dt = 6Dt, \tag{D1}$$

where D is the self-diffusion coefficient of the molecules and $d_{\rm s}$ is the space dimension (Here, $d_{\rm s} = 3$). Let us define the time required for the molecules to diffuse by their size as the translational diffusion time $\tau_{\rm t} = 1/6D$ [62]. We fitted the mean-squared displacements for the molecules A and B with Eq. (D1) to obtain the self-diffusion coefficients D and their corresponding times $\tau_{\rm t}$. Figure 16 is the translational diffusion times of the molecules A and B as functions of temperature. The system is the homogeneous binary quadrupolar fluids with $|Q| = 4.32 \times 10^{-2}$, $N = 16,384$, and $x_{\rm A} = 0.5$. We observe that the characteristic times are always much larger than the time mesh width $\Delta t = 0.005$.

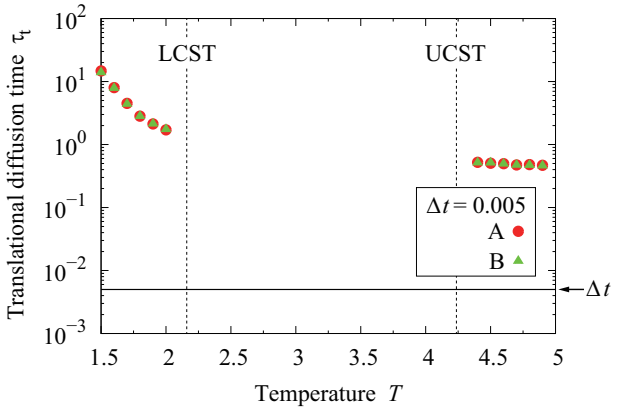

FIG. 16. (Color online) Temperature dependence of translational diffusion times $\tau_{\rm t}$ of the molecular centers for the binary system with $|Q| = 4.32 \times 10^{-2}$, $N = 16,384$, and $x_{\rm A} = 0.5$. Red filled circles and green filled triangles correspond to the characteristic times of the molecules A and B, respectively. The arrow indicates the time mesh width $\Delta t = 0.005$.

Similarly, when the rotational motions of the directors are mutually uncorrelated and randomly fluctuated, we can get a simple analytic expression for the time-correlation function [61]:

$$\langle \mathbf{u}(t) \cdot \mathbf{u}(0)\rangle = \exp\left[-\frac{t}{\tau_{\rm r}}\right], \tag{D2}$$

where $\tau_{\rm r}$ is the rotational correlation time. Figure 17 is the time-correlation functions for the molecules A and B in the binary fluid with $|Q| = 4.32 \times 10^{-2}$. We set $x_{\rm A} = 0.5$ and $T = 1.8$ ($<$ LCST). Both curves show a monotonic decrease. Although they do not show an exact single exponential decay because of the many-body correlation between the directors, we tried to fit them with Eq. (D2) and we obtained the characteristic time $\tau_{\rm r} = 7.0$, which is much larger than the time mesh width Δt. As our choice $\Delta t = 0.005$ satisfies the relations $\tau_{\rm t} \gg \Delta t$ and $\tau_{\rm r} \gg \Delta t$, we conclude that our choice of Δt is justified.

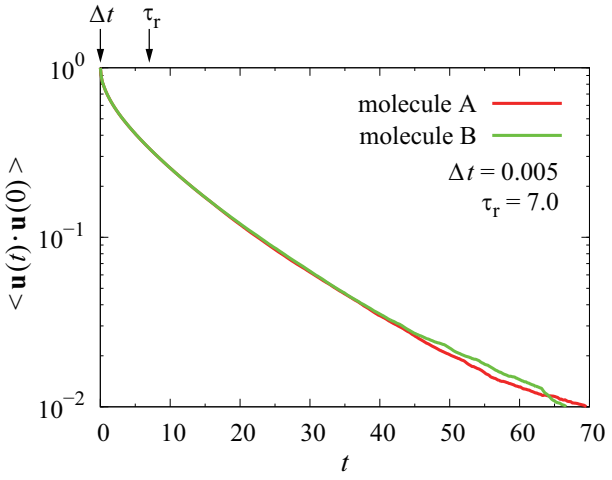

FIG. 17. (Color online) Orientational correlation functions $\langle \mathbf{u}(t) \cdot \mathbf{u}(0)\rangle$ of the directors $\mathbf{u}(t)$ embedded in the molecules A (red curve) and B (green one) for the equimolar binary mixture with $|Q| = 4.32 \times 10^{-2}$ and $N = 16,384$ at $T = 1.8$ ($<$ LCST). These curves are plotted in semilogarithmic scales. Two arrows indicate the time mesh width $\Delta t = 0.005$ and the time constant $\tau_{\rm r} = 7.0$.

Appendix E: The radial distribution function and the coordination number

We need to set a threshold value of the inter-charge distance in order to define the short-ranged anisotropic bond between two electric charges with the opposite signs belonging to different types of molecules. For that purpose, we make use of the radial distribution function $g(r)$ between the two electric charges and its integral, *i.e.*, the coordination number

$$N(r) \equiv \rho_{\rm e} \int_0^r g(u)\, 4\pi u^2\, {\rm d}u. \tag{E1}$$

Here, $\rho_{\rm e}$ is the number density of one species of the charge pair. Figure 18 shows $g(r)$ and $N(r)$ between $+q$ in a molecule A and $-q$ in a molecule B (see also Fig. 2), which are obtained from MD simulations for the binary system with $|Q| = 4.32 \times 10^{-2}$, $N = 16,384$, and $x_{\rm A} = 0.5$. The temperature changes from $T = 1.5$ to 2.0 ($<$ LCST) and from $T = 4.4$ to 4.9 ($>$ UCST). Both $g(r)$ and $N(r)$ are sensitive to the temperature when $T <$ LCST, while they are almost independent of the temperature when $T >$ UCST. We define $r = 0.60$ as the threshold value based on the shapes of $g(r)$ and $N(r)$ at $T = 1.5$ (solid blue curves). This value corresponds to a point on a dip between the first and second peaks of $g(r)$ and a point on a flat region of $N(r)$. The coordination number $N(r = 0.60) \simeq 0.85$ at $T = 1.5$ indicates that the short-ranged bonds are almost pair-wise, which is reminiscent of the hydrogen bond. The number of the charges $+q$ in the molecule A is two, so that we can interpret that the functionality per quadrupolar molecule at low temperatures is about two. Finally, we comment that the functions $g(r)$ and $N(r)$ quantitatively coincide with those obtained from GEMC simulations.

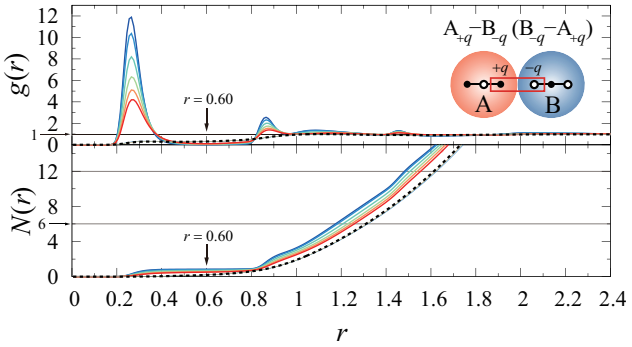

FIG. 18. (Color online) The radial distribution function $g(r)$ and the coordination number $N(r)$ as functions of a radial distance r between two charges with the opposite signs belonging to different types of molecules ($+q$ in a molecule A and $-q$ in a molecule B) for the binary system with $|Q| = 4.32 \times 10^{-2}$ and $N = 16,384$. The composition is equimolar ($x_{\rm A} = 0.5$). The temperature changes from $T = 1.5$ to 2.0 ($<$ LCST) and from $T = 4.4$ to 4.9 ($>$ UCST). In the former case, several curves are expressed with solid colored ones. In the latter case, on the other hand, all the curves are almost overlapped. Among the overlapped curves, we draw $g(r)$ and $N(r)$ at $T = 4.9$ with the dashed black curves. The distance $r = 0.60$ indicated by the arrows are the threshold used in the definition of the short-ranged anisotropic bonds.

[1] J. S. Rowlinson and F. L. Swinton, *Liquids and Liquid Mixtures*, 3rd ed., Butterworths Monographs in Chemistry (Butterworth Scientific, 1982).
[2] A. W. Francis, *Critical Solution Temperatures*, Adv. Chem. Ser. No. 31 (ACS, 1961).
[3] C. S. Hudson, Z. Phys. Chem. **47**, 113 (1904).
[4] T. Narayanan and A. Kumar, Phys. Rep. **249**, 135 (1994).
[5] A. Reinhardt, A. J. Williamson, J. P. K. Doye, J. Carrete, L. M. Varela, and A. A. Louis, J. Chem. Phys. **134**, 104905 (2011).
[6] F. Zhang, F. Roosen-Runge, A. Sauter, M. Wolf, R. M. J. Jacobs, and F. Schreiber, Pure Appl. Chem. **86**, 191 (2014).
[7] N. Altamirano, D. Kubizňák, and R. B. Mann, Phys. Rev. D **88**, 101502(R) (2013).
[8] J. S. Walker and C. A. Vause, Sci. Am. **255**, 90 (1987).
[9] S. C. Glotzer and M. J. Solomon, Nature Materials **6**, 557 (2007).
[10] J. C. Wheeler, Ann. Rev. Phys. Chem. **28**, 411 (1977).
[11] M. Kotelyanskii, B. Veytsman, and S. K. Kumar, Phys. Rev. E **58**, R12 (1998).
[12] L. A. Davies, G. Jackson, and L. F. Rull, Phys. Rev. Lett. **82**, 5285 (1999).
[13] A. Z. Panagiotopoulos, Mol. Phys. **61**, 813 (1987).
[14] A. Z. Panagiotopoulos, J. Phys.: Condens. Matter **12**, R25 (2000).
[15] D. Frenkel and B. Smit, *Understanding Molecular Simulation: From Algorithms to Applications*, 2nd ed. (Academic Press, 2001).
[16] M. P. Allen and D. J. Tildesley, *Computer Simulation of Liquids* (Oxford University Press, Oxford, 1989).
[17] J. D. Weeks, D. Chandler, and H. C. Andersen, J. Chem. Phys. **54**, 5237 (1971).
[18] A. D. McLean and M. Yoshimine, J. Chem. Phys. **47**, 1927 (1967).
[19] W. L. Jorgensen, J. Chandrasekhar, J. D. Madura, R. W. Impey, and M. L. Klein, J. Chem. Phys. **79**, 926 (1983).
[20] J. O. Hirschfelder, C. F. Curtiss, and R. B. Bird, *Molecular Theory of Gases and Liquids*, 1st ed. (Wiley, 1964).
[21] K. VanWorkum and J. F. Douglas, Phys. Rev. E **71**, 031502 (2005).
[22] G. C. Maitland, M. Rigby, E. B. Smith, and W. A. Wakeham, *Intermolecular Forces: Their Origin and Determination* (Clarendon Press, Oxford, 1981).
[23] R. Koningsveld, W. H. Stockmayer, and E. Nies, *Polymer Phase Diagrams* (Oxford University Press, 2001).
[24] L. A. Rowley, D. Nicholson, and N. G. Parsonage, J. Comput. Phys. **17**, 401 (1975).

[25] J. Yao, R. A. Greenkorn, and K. C. Chao, Mol. Phys. **46**, 587 (1982).
[26] M. Mezei, Mol. Phys. **40**, 901 (1980).
[27] A. Z. Panagiotopoulos, Int. J. Thermophys. **10**, 447 (1989).
[28] S. K. Das, J. Horbach, and K. Binder, J. Chem. Phys. **119**, 1547 (2003).
[29] S. K. Das, M. E. Fisher, J. V. Sengers, J. Horbach, and K. Binder, Phys. Rev. Lett. **97**, 025702 (2006).
[30] S. K. Das, J. Horbach, K. Binder, M. E. Fisher, and J. V. Sengers, J. Chem. Phys. **125**, 024506 (2006).
[31] D. A. Kofke and E. D. Glandt, Mol. Phys. **64**, 1105 (1988).
[32] H. C. Andersen, J. Comput. Phys. **52**, 24 (1983).
[33] G. Ciccotti and J. P. Ryckaert, Comput. Phys. Rep. **4**, 345 (1986).
[34] H. J. C. Berendsen and W. F. van Gunsteren, in *Molecular Liquids—Dynamics and Interactions*, edited by A. J. Barnes, W. J. Orville-Thomas, and J. Yarwood (D. Reidel Publishing Company, Dordrecht, 1984) pp. 475–500.
[35] K. A. Feenstra, B. Hess, and H. J. C. Berendsen, J. Comput. Chem. **20**, 786 (1999).
[36] L. V. Woodcock, Chem. Phys. Lett. **10**, 257 (1971).
[37] P. H. Hünenberger, Adv. Polym. Sci. **173**, 105 (2005).
[38] A. Arnold and C. Holm, Adv. Polym. Sci. **185**, 59 (2005).
[39] M. J. L. Sangster and M. Dixon, Adv. Phys. **25**, 247 (1976).
[40] R. W. Hockney and J. W. Eastwood, *Computer Simulation Using Particles* (McGraw-Hill Inc., New York, 1981).
[41] M. Deserno and C. Holm, J. Chem. Phys. **109**, 7678 (1998).
[42] M. Deserno and C. Holm, J. Chem. Phys. **109**, 7694 (1998).
[43] V. Ballenegger, J. J. Cerda, O. Lenz, and C. Holm, J. Chem. Phys. **128**, 034109 (2008).
[44] H. E. Stanley, *Introduction to Phase Transitions and Critical Phenomena*, International Series of Monographs on Physics (Oxford University Press, 1987).
[45] R. Hentschke, J. Bartke, and F. Pesth, Phys. Rev. E **75**, 011506 (2007).
[46] J. Bartke and R. Hentschke, Phys. Rev. E **75**, 061503 (2007).
[47] M. R. Stapleton, D. J. Tildesley, A. Z. Panagiotopoulos, and N. Quirke, Mol. Sim. **2**, 147 (1989).
[48] C. F. Fan, B. D. Olafson, M. Blanco, and S. L. Hsu, Macromolecules **25**, 3667 (1992).
[49] W. H. Press, S. A. Teukolsky, W. T. Vetterling, and B. P. Flannery, *Numerical Recipes: The Art of Scientific Computing*, 3rd ed. (Cambridge University Press, 2007).
[50] M. Rubinstein and R. H. Colby, *Polymer Physics* (*Chemistry*) (Oxford University Press, 2003).
[51] F. Tanaka, *Polymer Physics: Applications to Molecular Association and Thermoreversible Gelation* (Cambridge University Press, 2011).
[52] I. Szalai and S. Dietrich, Mol. Phys. **103**, 2873 (2005).
[53] A. Goyal, C. K. Hall, and O. D. Velev, J. Chem. Phys. **133**, 064511 (2010).
[54] A. Onuki, *Phase Transition Dynamics* (Cambridge University Press, 2002).
[55] D. Stauffer and A. Aharony, *Introduction to Percolation Theory*, revised 2nd ed. (Taylor & Francis, 1994).
[56] F. Tanaka, Polym. J. **34**, 479 (2002).
[57] M. Matsumoto, A. Baba, and I. Ohmine, J. Chem. Phys. **127**, 134504 (2007).
[58] A. Onuki, J. Phys.: Condens. Matter **9**, 6119 (1997).
[59] N. Clarke, Adv. Polym. Sci. **183**, 127 (2005).
[60] D. J. Evans and G. Morriss, *Statistical Mechanics of Nonequilibrium Liquids*, 2nd ed. (Cambridge University Press, 2008).
[61] M. Doi and S. F. Edwards, *The Theory of Polymer Dynamics* (Clarendon Press, Oxford, 1986).
[62] L. D. Landau and E. M. Lifshitz, *Fluid Mechanics* (Pergamon, New York, 1959).

TABLE I. Numerical data of the two-phase coexistence curve ($x_{\mathrm{A,\,I}}$, T) of the binary quadrupolar mixtures at several magnitudes $|Q|$ obtained from GEMC simulations. The relation $x_{\mathrm{A,\,I}} = 1 - x_{\mathrm{A,\,II}}$ is satisfied exactly, because the constituent molecules of the binary system are completely symmetric and equimolar. The estimated error of $x_{\mathrm{A,\,I}}$ indicates the standard deviation.

	$x_{\mathrm{A,\,I}}$				
T	$\|Q\| = 0$	3.96×10^{-2}	4.10×10^{-2}	4.32×10^{-2}	4.41×10^{-2}
1.5		0.0277 ± 0.0055			
1.6	0.0004 ± 0.0008	0.0243 ± 0.0056	0.1316 ± 0.0157		
1.8	0.0013 ± 0.0014	0.0200 ± 0.0050	0.0612 ± 0.0088		
2.0	0.0035 ± 0.0021	0.0222 ± 0.0054	0.0460 ± 0.0078		
2.2	0.0066 ± 0.0028	0.0253 ± 0.0054	0.0460 ± 0.0080	0.3071 ± 0.0420	
2.3				0.2229 ± 0.0290	
2.4	0.0109 ± 0.0037	0.0309 ± 0.0066	0.0474 ± 0.0087	0.1596 ± 0.0203	
2.6	0.0161 ± 0.0044	0.0376 ± 0.0073	0.0530 ± 0.0089	0.1323 ± 0.0175	0.2981 ± 0.0388
2.7					0.2813 ± 0.0486
2.8	0.0234 ± 0.0057	0.0469 ± 0.0087	0.0623 ± 0.0098	0.1278 ± 0.0175	0.2337 ± 0.0357
2.9					0.2231 ± 0.0329
3.0	0.0319 ± 0.0067	0.0586 ± 0.0098	0.0740 ± 0.0114	0.1343 ± 0.0174	0.2136 ± 0.0349
3.1					0.2196 ± 0.0428
3.2	0.0432 ± 0.0081	0.0721 ± 0.0112	0.0879 ± 0.0134	0.1457 ± 0.0209	0.2125 ± 0.0310
3.3					0.2171 ± 0.0357
3.4	0.0565 ± 0.0091	0.0902 ± 0.0139	0.1079 ± 0.0165	0.1641 ± 0.0219	0.2333 ± 0.0380
3.5					0.2391 ± 0.0374
3.6	0.0728 ± 0.0111	0.1131 ± 0.0167	0.1295 ± 0.0183	0.1921 ± 0.0289	0.2523 ± 0.0367
3.7			0.1448 ± 0.0205		0.2743 ± 0.0480
3.8	0.0933 ± 0.0142	0.1377 ± 0.0197	0.1584 ± 0.0220	0.2275 ± 0.0362	0.3052 ± 0.0578
3.9			0.1772 ± 0.0254	0.2521 ± 0.0422	0.3396 ± 0.0754
4.0	0.1171 ± 0.0173	0.1723 ± 0.0247	0.1979 ± 0.0306	0.2849 ± 0.0507	
4.1	0.1315 ± 0.0190	0.1919 ± 0.0297	0.2223 ± 0.0348	0.3160 ± 0.0673	
4.2	0.1467 ± 0.0219	0.2161 ± 0.0366	0.2540 ± 0.0442	0.3723 ± 0.0768	
4.3	0.1656 ± 0.0242	0.2383 ± 0.0363	0.2769 ± 0.0473		
4.4	0.1877 ± 0.0289	0.2732 ± 0.0463	0.3205 ± 0.0610		
4.5	0.2144 ± 0.0348	0.3200 ± 0.0684			
4.6	0.2379 ± 0.0388				
4.7	0.2699 ± 0.0456				
4.8	0.3273 ± 0.0761				

TABLE II. Estimated critical temperatures of the binary quadrupolar mixtures at several magnitudes $|Q|$.

$\|Q\|$	LCST	UCST
0	No	4.88
3.96×10^{-2}	< 1.5 or No	4.60
4.10×10^{-2}	1.57	4.48
4.32×10^{-2}	2.16	4.24
4.41×10^{-2}	2.46	4.01